Near-Unity Indistinguishability Single Photon Source for Large-Scale Integrated Quantum Optics

Łukasz Dusanowski,[1,*] Soon-Hong Kwon,[1,2] Christian Schneider,[1] and Sven Höfling[1,3]
[1]Technische Physik, University of Würzburg, Physikalisches Institut and Wilhelm-Conrad-Röntgen-Research Center for Complex Material Systems, Am Hubland, D-97074 Würzburg, Germany
[2]Department of Physics, Chung-Ang University, 156-756 Seoul, Korea
[3]SUPA, School of Physics and Astronomy, University of St Andrews, KY16 9SS St Andrews, United Kingdom

(Received 21 June 2018; revised manuscript received 9 January 2019; published 3 May 2019)

Integrated single photon sources are key building blocks for realizing scalable devices for quantum information processing. For such applications highly coherent and indistinguishable single photons on a chip are required. Here we report on a triggered resonance fluorescence single photon source based on In(Ga)As/GaAs quantum dots coupled to single- and multimode ridge waveguides. We demonstrate the generation of highly linearly polarized resonance fluorescence photons with 99.1% (96.0%) single photon purity and 97.5% (95.0%) indistinguishability in case of multimode (single mode) waveguide devices fulfilling the strict requirements imposed by multi-interferometric quantum optics applications. Our integrated triggered single photon source can be readily scaled up, promising a realistic pathway for on-chip linear optical quantum simulation, quantum computation, and quantum networks.

DOI: 10.1103/PhysRevLett.122.173602

Large scale implementations of quantum information processing (QIP) schemes are one of the major challenges of modern quantum physics. Building a platform successfully combing many qubits is a very demanding task; however, it would provide a system capable to perform quantum simulations, quantum computing, and secure quantum communication. In this regard, using single photons as qubits is a particularly appealing concept. Because of the photons' low decoherence and the inherent possibility of low-loss transmission, they can be used for both quantum computing and quantum communication applications [1]. Over the last decade, there have been extensive experimental efforts toward realizing large-scale optical QIP systems. A vast majority of these implementations, such as linear optics quantum computing [2], boson sampling [3], or quantum repeater schemes [4] involve a two-photon interference effect, where a complete wave-packet overlap of single photons at the beam splitter is required. This feature demands photons, which are indistinguishable in terms of energy, bandwidth, polarization, and arrival time at the beam splitter. Consequently, sources of indistinguishable single photons are one of the central resources for a large scale experimental realization of the optical QIP devices.

Among different kinds of emitters quantum dots (QDs) coupled to photonic structures have been shown to be one of the brightest single photon sources (SPSs) [5–7], which under resonant excitation conditions [7–9] can reach simultaneously indistinguishabilities higher than 95%, single photon purities better than 99%, and extraction efficiencies as high as 65%–79% [7,10–13]. Further, by applying advanced semiconductor microprocessing technologies, it is possible to fabricate devices where QD electronic properties can be dynamically shaped by strain [14,15] or electric [16,17] fields. The optical quality of such sources allowed already for demonstration of on-demand CNOT gates [18–20] heralded entanglement between distant hole spins [21] or the recent realization of three-, four-, and five-photon boson sampling [22,23].

It is believed that future steps toward large scale quantum optics should ensure the full on-chip scalability of SPSs [6,24]. A natural system toward this goal are integrated circuits, where QD SPSs can be homogeneously [25–29] or heterogeneously [30–32] integrated on a single chip. In this approach, light can be directly coupled into in-plane waveguides (WGs) and combined with other functionalities on a chip such as phase shifters [33,34], beam splitters [25,32,35], filters [31,36], detectors [29,37], and other devices for light propagation, manipulation, and detection on a single photon level.

By utilizing this idea near-unity coupling efficiency of a QD emitter to waveguide device was already achieved [26,28,38,39], showing the undeniable potential of this concept. In addition, integrated circuits allow us to spatially separate excitation and detection spots, which straightforwardly enables applying resonant driving schemes to slow-down decoherence processes and reduce on-demand emission time jitter. This technique was already applied to waveguide integrated QDs under both continuous-wave [40,41] (CW) and pulsed [16,42,43] excitation. In particular, two-photon interference of subsequently emitted resonance fluorescence photons have been demonstrated recently [16,43]; however, recorded indistinguishability

values failed to reach requirements imposed by quantum optics applications [44].

One of the major issues in QD-based on-chip SPSs is the loss of photon indistinguishability related to the charge fluctuation from nearby etched surfaces [40,41]. This is true especially for small in size, complex structures such as photonic crystal [43] or nanobeam [16] waveguides. To diminish this effect, a number of strategies can be employed. First, the amount of surface states could be decreased by optimizing passivation of the etched surfaces [45]. Second, the charge environment could be stabilized by weak CW nonresonant optical illumination [46] or gating [11,43]. Finally, the Purcell effect might be used to enhance the radiative emission rate and thus improve the photon indistinguishability in the presence of dephasing [10–12,43,47]. As we will show in this Letter, a simplified waveguide design with relatively large profile dimensions, keeping etched surfaces far away from QD, can be also very advantageous in this respect. By utilizing distributed Bragg reflectors (DBR) ridge waveguide design, we fabricated SPSs which simultaneously meet the requirements of near perfect single photon purity and indistinguishability.

To evaluate the performance of our devices, we performed resonance fluorescence experiments on In(Ga)As/GaAs QDs coupled to single mode (SM) and multimode (MM) in-plane waveguides. The light confinement and guiding were achieved by DBRs in vertical and ridges defined in horizontal direction. Usage of DBRs WG instead of the GaAs WG slab approach allowed us to soften the waveguide profile dimensions allowing us to achieve single mode operation while keeping a relatively high QD-waveguide light coupling efficiency (14%–19% into one WG arm). To simulate the integrated circuit device operation, the QDs were excited resonantly from top of the waveguides, and the emitted photons were collected from the side facets after up to 1 mm travel distance on a chip. Under such conditions, a significant reduction of the scattered laser intensity was achieved, enabling our MM (SM) waveguide device generation of record high on-chip 97.5% (95.0%) indistinguishable triggered single photons with a 99.1% (96.0%) single photon purity and over 99% (98%) linear polarization. We believe, that this integrated SPSs can be readily scaled up demonstrating a realistic pathway for on-chip optical quantum processing.

To realize our waveguide integrated SPS, we have grown In(Ga)As/GaAs QDs embedded in a low-quality factor cavity ($Q \sim 200$) based on DBRs. By performing three-dimensional finite-difference-time-domain calculations we investigated different waveguide designs for maximized coupling efficiency. We found that 1.25–1.65 μm WG height and 0.6–2.0 μm width lay within optimal values and allowed us to achieve around 10%–22% coupling efficiency into each WG arm (total 20%–44%). Moreover, our DBR waveguides can be operated in the single mode regime for WG widths as small as 0.9 μm at 900 nm cutoff wavelengths. Based on those considerations, we realized two types of ridge waveguides: (i) MM WGs with 2.0×1.25 μm^2 profile and (ii) SM WGs with 0.8×1.25 μm^2, for which we expect ~14% and ~19% QD coupling efficiency into one WG arm, respectively. We point out, that in principle the QD-emission coupling efficiency could be further improved by integration of DBR WGs with low-refractive-index layers while maintaining the mentioned relatively large size of WG profile. More details can be found in the Supplemental Material [48]. Scanning electron microscope images of our fabricated MM and SM ridge waveguides are shown in Figs. 1(a) and 1(c), respectively. Figures 1(b) and 1(d) show simulated optical mode profiles of the light field confined in our devices, calculated for the transverse-electric (TE) modes at 930 nm. In both cases, the mode profiles are confined within the defined ridges, allowing for the single photon guiding along the chip. The modes are mainly concentrated in the GaAs cores and partially penetrate the top and bottom DBR mirrors.

Initially, both devices were characterized optically under nonresonant excitation conditions. Figures 2(a) and 2(c) show side collected photoluminescence (PL) spectra from a QD_1 and QD_2, respectively, under above-band-gap CW pump (660 nm diode laser) from the top of the waveguide. In case of QD_1 coupled to an MM WG four intense emission lines are visible, where the one of interest centered at 1.3169 eV (marked with an arrow) was identified as a neutral exciton (X). The inset in Fig. 2(a) shows central peak intensity changes vs excitation power indicating a clear linear dependence. The remaining emission lines have been identified based on power- and top-detected-polarization-resolved PL as positively charged exciton (X^+), negatively charged exciton (X^-), and biexciton (XX) recombination from the same QD. Spectra for QD_2 coupled to the SM WG consists of a single emission line centered at 1.3206 eV, identified as a charged exciton (CX). Both studied emission lines show a high degree of linear

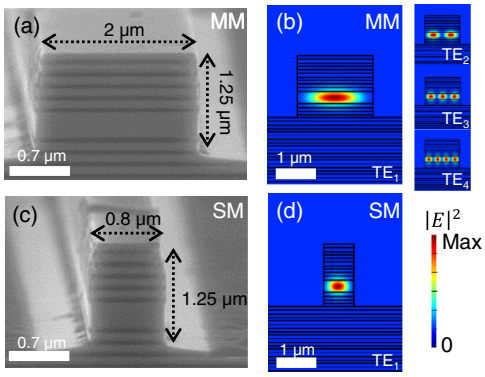

FIG. 1. Ridge waveguide image and mode profile. Scanning electron microscope images of the processed (a) multimode (MM) and (c) single mode (SM) ridge waveguide structure. Optical power distribution profile for the TE (b) fundamental —TE_1 and higher order—TE_{2-4} modes of MM and (d) fundamental TE_1 mode of SM waveguide at 930 nm wavelength.

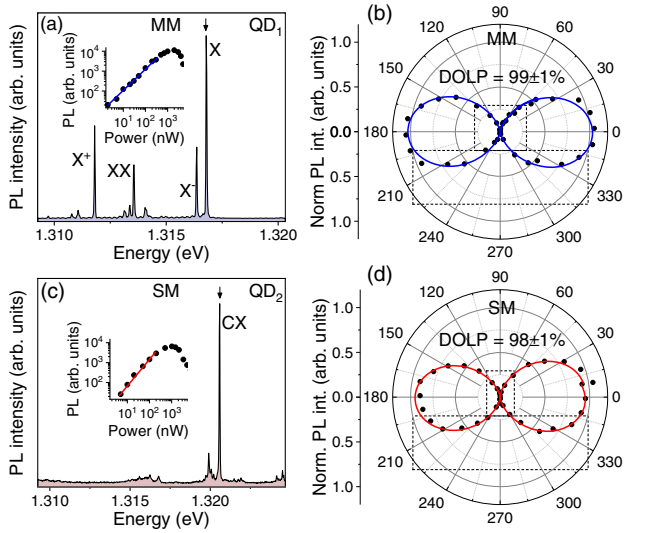

FIG. 2. Nonresonant photoluminescence. Side collected QD emission spectra recorded from (a) MM and (c) SM ridge WG device at 1 μW power CW excitation. Insets: intensity vs power dependencies of the marked with arrows PL peaks in log-log scale. Red/blue solid curve: fit with a power function showing linear dependence. Polarization characteristics of the (b) MM and (d) SM WG coupled QD PL emission, revealing $99 \pm 1\%$ and $98 \pm 1\%$ degree of linear polarization, respectively, oriented along the TE mode of the ridge waveguides.

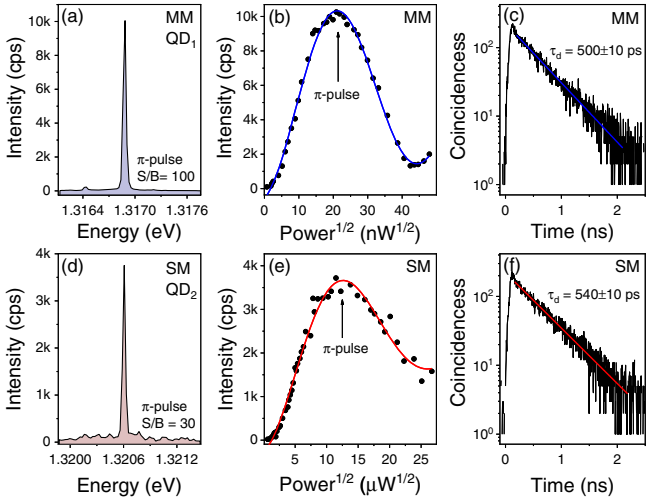

FIG. 3. Pulsed resonance fluorescence. Side collected QD emission spectra from (a) MM and (d) SM waveguide device under π-pulse excitation. (b),(e) Signal intensity vs square root of incident power. Solid red/blue curve: fit with a dumped sinusoidal function. (c),(f) Time-resolved resonance fluorescence measurement under π-pulse pumping. Red/blue solid curves: fit using a monoexponential decay function with time constants of 500 ± 10 and 540 ± 10 ps for MM and SM devices, respectively.

polarization (DOLP) of around $99 \pm 1\%$ and $98 \pm 1\%$ for QD_1 and QD_2, respectively, oriented in sample plane as shown in Figs. 2(b) and 2(d). A high DOLP and its direction are related to the QDs dipole moments, which are mainly in-plane oriented and thus emitted photons mostly couple to and propagate in the TE waveguide mode.

Next, the characteristics of the devices were probed under pulsed *s*-shell resonant excitation. Figures 3(a) and 3(d) show side detected pulsed resonance fluorescence spectra displayed on a spectrometer at a temperature of 4.5 K. Because in our experimental configuration the excitation and collection spots are spatially separated by hundreds of micrometers, it allows us to rather readily suppress the stray laser photons scattered from the excitation area. This is usually not the case for short length waveguides because the laser light scattered from the excitation area might be collected within the numerical aperture of the detection objective. Additionally, the presence of low Q factor cavity in the plane of the sample allowed us to more effectively excite the emitters and thus reduce powers needed for resonant driving. To further suppress the influence of laser light scattering on the single photon performance, the beam spot size, as well as polarization, was carefully controlled. By utilizing both the intrinsic (spatial separation) and polarization filtering, we were able to obtain a signal-to-background (S/B) ratio of over 100 for MM and 30 for SM waveguide devices under π-pulse excitation. In fact, we believe that polarization filtering can be omitted for fully on-chip device operation.

In Figs. 3(b) and 3(e), the resonance fluorescence intensity vs the square root of the incident power is shown. Clear Rabi oscillations with visible damping for both QDs are observed, which is due to coherent control of the particular QD's two-level systems coupled to phonon bath [49]. The emission intensities in both cases reach the maximum for π pulse with laser powers of 440 nW and 160 μW for QD_1 and QD_2, respectively. The significantly larger pump power required to reach π pulse for QD_2 is most likely related to the smaller size of the waveguide in respect to the laser beam spot size, as well as a slight energy detuning from the planar cavity resonance. The resonance fluorescence intensity of around 10 kcps (3.5 kcps) was observed on the avalanche photodiode detector (setup efficiency ~2%) at π pulse for an MM (SM) device, which corresponds to ~0.6% (~0.2%) total photon extraction efficiency from a QD collected by the first lens, and ~12% (~2%) coupling efficiency into one WG arm (lower bound estimated based on 95% and 90% losses due to the out-coupling). It needs to be noted that the design of the WGs for the high out-coupling into external collection optics was not optimized since ultimately all single photon processing is supposed to be performed on-chip. Under π-pulse excitation, the time-resolved resonance fluorescence measurements have been performed. The recorded fluorescence decay time traces shown in Figs. 3(c) and 3(f) demonstrate clear monoexponential decays with the time constants of 500 ± 10 and 540 ± 10 ps for QD_1 and QD_2, respectively.

In order to characterize purity and indistinguishability of our SPSs, autocorrelation and two-photon interference

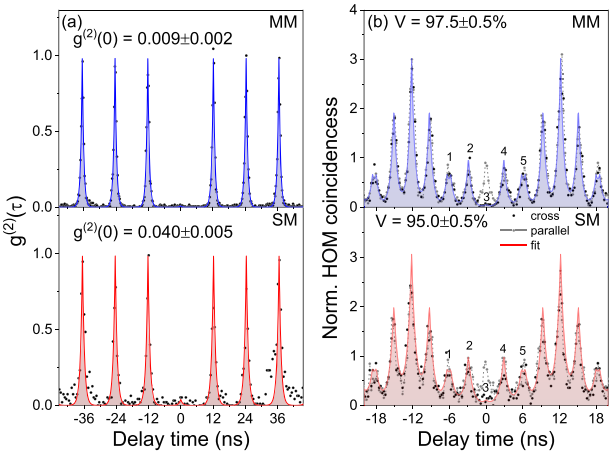

FIG. 4. Single photon generation and two photon interference under resonant π-pulse excitation. (a) Side collected resonance fluorescence intensity-correlation histogram recorded for QD_1 coupled to MM WG (upper panel) and QD_2 coupled to SM WG (lower panel). $g^{(2)}(0)$ values are calculated from the integrated photon counts, while the uncertainty is based on the standard deviation of the Poissonian peak counts. (b) Two-photon interference HOM histogram recorded for the 3 ns time separated co- (black points) and cross-polarized (grey points) single photons recorded for QD_1 (upper panel) and QD_2 (lower panel). Red/blue solid curves: fits based on two-sided exponential decay functions.

experiments have been performed on the resonance fluorescence signal filtered out from a broader laser profile and phonon sidebands. In Fig. 4(a), second-order correlation function histograms recorded in Hanbury Brown and Twiss (HBT) configuration under π-pulse excitation for QD_1 and QD_2 are shown. In both cases, nearly vanishing multiphoton emission probabilities at zero delays have been recorded with $g^{(2)}(0) = 0.009 \pm 0.002$ and $g^{(2)}(0) = 0.040 \pm 0.005$ for QD_1 and QD_2, respectively. The shape of all the peaks exhibits a clear two-sided monoexponential decay with a time constant corresponding to the decay time recorded directly in the time-resolved resonance fluorescence measurements.

To study the indistinguishability of the emitted photons, the QDs were excited twice every repetition cycle (12.2 ns) by a pair of pulses separated by 3 ns. Two subsequently emitted photons are then introduced into a 3-ns unbalanced interferometer where a delay between them is compensated in order to superimpose single photon pulses on the beam splitter [5]. If the two photons are perfectly indistinguishable, they will always exit the same but a random output port, which is quantitatively translated into the two-coincidences correlation dip at a zero delay. Hong-Ou-Mandel (HOM) correlation histograms obtained for the two considered photon sources are presented in Fig. 4(b) in upper (QD_1) and lower (QD_2) panels. The histograms consist of a set of five 3 ns delayed peak clusters separated by the repetition time of the laser (first and the last peaks of the neighboring clusters are superimposed). The central cluster describes coincidence events related to the single photons traveling through different paths of the interferometer. This is described in detail in the Supplemental Material [48]. In order to evaluate the zero delay peak (no. 3) area with respect to the neighboring peaks (no. 2 and 4), the experimental data have been fitted with the two-side exponential decay functions. Upon this procedure, the two-photon HOM interference visibility of 0.975 ± 0.005 for QD_1 and 0.950 ± 0.005 for QD_2 have been obtained after correcting for HOM setup imperfections such as beam-splitting ratio ($R/T = 1.15$) and contrast of the Mach-Zehnder interferometer ($1 - \varepsilon = 0.99$) [5,13].

It was recently demonstrated, that single photon emission purity and indistinguishability in resonantly excited two-level systems is intrinsically limited by the re-excitation process [13,50]. Specifically, it was shown that the laser excitation pulse-length τ_{pulse} sets the lower bounds of the HBT and HOM experimental two-photon coincidences probability, and thus $g^{(2)}(0)$ and visibility values obtainable for a given SPS with characteristic emission time τ_{emitter}. Based on Ref. [13], those bounds can be calculated following the linear dependence $0.4 \cdot \tau_{\text{pulse}}/\tau_{\text{emitter}}$, which in our case limits $g^{(2)}(0)$ (visibility) to 0.0016 (0.9984) and 0.0015 (0.9985) for QD_1 and QD_2, respectively. Because the experimentally obtained single photon purity values are significantly above the aforementioned limits, we believe their dominant component might be nonfiltered residual scatter of the laser pulse from the sample surface, which we do not take into account in HBT and HOM data analysis.

Imperfect efficiency and indistinguishability of SPSs are related to the problem of optical quantum computation under a degree of experimental error. There have been a number of promising proposals of linear optical quantum computing that are robust against imperfect SPSs and inefficient detectors. In particular, it was shown, that fault-tolerant quantum computation can be performed if the two-photon gate operation error probability is lower than a 1% threshold value [51,52]. In this regard, we can calculate how the indistinguishability of input photons affects the two-photon gate performance assuming perfect beam overlap, alignment, beam splitters, and no dark counts in single photon counting detection. In case of our MM (SM) waveguide QD source with 97.5% (95.0%) photons visibility, a gate fidelity of 99.5% (99.1%) [53] is theoretically obtainable. Those values already surpass mentioned 1% precision threshold value, and in this context, our work provides SPSs with photons visibility needed for scalable quantum technologies.

Another source of error in quantum optics, which is far more dominant than gate fidelity, is photon loss. This problem is associated with the overall source and detectors efficiency, which product has to be greater than $2/3$ in order to perform efficient fault-tolerant linear optical quantum computation [54]. In principle, this efficiency threshold is

very difficult to fulfill in any system, because every optical setup exhibit losses. In all on-chip platforms however, where single photons are generated, routed, manipulated, and eventually detected within the same low loss photonic circuit, this efficiency threshold is likely to be fulfilled within the near future.

In this context, essential next steps to make QD-based on-chip platform feasible for fully scalable quantum technologies would consist of (i) improving QD-waveguide circuit coupling efficiency while maintaining high degree of photons indistinguishability, (ii) introducing high-visibility and low-loss on-chip interferometers and phase shifters based on single mode waveguides, and (iii) integrating with high efficiency superconducting detectors [6,7,24]. Such a system may at some point overcome the intrinsic limitations of the vertical devices, opening the possibility to create a scalable quantum integrated circuits operating at the single photon level.

In this Letter, we have shown that our MM (SM) waveguide integrated SPS can generate photons with near-unity indistinguishability of 0.975 ± 0.005 (0.950 ± 0.005) along with the $g^{(2)}(0)$ value equal to 0.009 ± 0.002 (0.040 ± 0.005). We demonstrated single photon propagation of over hundreds of micrometers in waveguides and QD-WG coupling efficiency of ∼12% (∼2%) into one WG arm. In contrast to any other QD-based waveguide integrated SPS which has been demonstrated thus far [16,43], our devices fulfill ultimate single photon purity and indistinguishability demands, imposed by boson sampling and linear optical quantum computing applications [44]. Performance of this source already outperforms any other on-chip integrated emitters including state-of-the-art heralded single photon spontaneous parametric down-conversion sources, where a maximum of 91% photons indistinguishability has been achieved at 4%–5% source efficiency [55,56]. We believe that our device could be straightforwardly integrated with advanced on-chip functionalities including reconfigurable and reprogrammable optical circuits [57] suitable for handling large scale multiphoton experiments. A potential of manufacturing such advanced quantum circuits combined with high purity indistinguishable SPS opens a route toward fully integrated and thus scalable quantum information processing.

The authors thank Silke Kuhn for fabricating the structures and Dominick Köck for calculating the electric field distribution in waveguides. Ł. D. acknowledges the financial support from the Alexander von Humboldt Foundation. S.-H. K. acknowledges the financial support from the National Research Foundation of Korea through the Korean Government Grant No. NRF-2016R1C1B2007007. We acknowledge funding by the German Research Foundation (DFG) within the Grants No. H05194/8-1 and No. SCHN1376-5.1. We are furthermore grateful for the support by the State of Bavaria.

*lukasz.dusanowski@physik.uni-wuerzburg.de

[1] P. Kok and B. Lovett, *Introduction to Optical Quantum Information Processing* (Cambridge University Press, Cambridge, United Kingdom, 2010), https://doi.org/10.1017/CBO9781139193658.
[2] E. Knill, R. Laflamme, and G. J. Milburn, Nature (London) **409**, 46 (2001).
[3] J. B. Spring, B. J. Metcalf, P. C. Humphreys, W. S. Kolthammer, X.-M. Jin, M. Barbieri, A. Datta, N. Thomas-Peter, N. K. Langford, D. Kundys, J. C. Gates, B. J. Smith, P. G. R. Smith, and I. A. Walmsley, Science **339**, 798 (2013).
[4] H.-J. Briegel, W. Dür, J. I. Cirac, and P. Zoller, Phys. Rev. Lett. **81**, 5932 (1998).
[5] C. Santori, D. Fattal, J. Vucković, G. S. Solomon, and Y. Yamamoto, Nature (London) **419**, 594 (2002).
[6] I. Aharonovich, D. Englund, and M. Toth, Nat. Photonics **10**, 631 (2016).
[7] P. Senellart, G. Solomon, and A. White, Nat. Nanotechnol. **12**, 1026 (2017).
[8] E. B. Flagg, A. Muller, J. W. Robertson, S. Founta, D. G. Deppe, M. Xiao, W. Ma, G. J. Salamo, and C. K. Shih, Nat. Phys. **5**, 203 (2009).
[9] S. Ates, S. M. Ulrich, S. Reitzenstein, A. Löffler, A. Forchel, and P. Michler, Phys. Rev. Lett. **103**, 167402 (2009).
[10] X. Ding, Y. He, Z. C. Duan, N. Gregersen, M. C. Chen, S. Unsleber, S. Maier, C. Schneider, M. Kamp, S. Höfling, C.-Y. Lu, and J.-W. Pan, Phys. Rev. Lett. **116**, 020401 (2016).
[11] N. Somaschi, V. Giesz, L. De Santis, J. C. Loredo, M. P. Almeida, G. Hornecker, S. L. Portalupi, T. Grange, C. Antón, J. Demory, C. Gómez, I. Sagnes, N. D. Lanzillotti-Kimura, A. Lemaître, A. Auffeves, A. G. White, L. Lanco, and P. Senellart, Nat. Photonics **10**, 340 (2016).
[12] S. Unsleber, Y.-M. He, S. Maier, S. Gerhardt, C.-Y. Lu, J.-W. Pan, M. Kamp, C. Schneider, and S. Höfling, Opt. Express **24**, 8539 (2016).
[13] K. A. Fischer, K. Müller, K. G. Lagoudakis, and J. Vučković, New J. Phys. **18**, 113053 (2016).
[14] Y. Zhang, Y. Chen, M. Mietschke, L. Zhang, F. Yuan, S. Abel, R. Hühne, K. Nielsch, J. Fompeyrine, F. Ding, and O. G. Schmidt, Nano Lett. **16**, 5785 (2016).
[15] R. Trotta, J. Martín-Sánchez, J. S. Wildmann, G. Piredda, M. Reindl, C. Schimpf, E. Zallo, S. Stroj, J. Edlinger, and A. Rastelli, Nat. Commun. **7**, 10375 (2016).
[16] G. Kiršanskė, H. Thyrrestrup, R. S. Daveau, C. L. Dreeßen, T. Pregnolato, L. Midolo, P. Tighineanu, A. Javadi, S. Stobbe, R. Schott, A. Ludwig, A. D. Wieck, S. I. Park, J. D. Song, A. V. Kuhlmann, I. Söllner, M. C. Löbl, R. J. Warburton, and P. Lodahl, Phys. Rev. B **96**, 165306 (2017).
[17] T. B. Hoang, J. Beetz, M. Lermer, L. Midolo, M. Kamp, S. Höfling, and A. Fiore, Opt. Express **20**, 21758 (2012).
[18] M. A. Pooley, D. J. P. Ellis, R. B. Patel, A. J. Bennett, K. H. A. Chan, I. Farrer, D. A. Ritchie, and A. J. Shields, Appl. Phys. Lett. **100**, 211103 (2012).
[19] O. Gazzano, M. P. Almeida, A. K. Nowak, S. L. Portalupi, A. Lemaître, I. Sagnes, A. G. White, and P. Senellart, Phys. Rev. Lett. **110**, 250501 (2013).
[20] Y.-M. He, Y. He, Y.-J. Wei, D. Wu, M. Atatüre, C. Schneider, S. Höfling, M. Kamp, C.-Y. Lu, and J.-W. Pan, Nat. Nanotechnol. **8**, 213 (2013).

[21] A. Delteil, Z. Sun, W.-b. Gao, E. Togan, S. Faelt, and A. Imamoglu, Nat. Phys. **12**, 218 (2016).

[22] H. Wang, Y.-M. He, Y.-H. Li, Z.-E. Su, B. Li, H.-L. Huang, X. Ding, M.-C. Chen, C. Liu, J. Qin, J.-P. Li, Y.-M. He, C. Schneider, M. Kamp, C.-Z. Peng, S. Höfling, C.-Y. Lu, and J.-W. Pan, Nat. Photonics **11**, 361 (2017).

[23] J. C. Loredo, M. A. Broome, P. Hilaire, O. Gazzano, I. Sagnes, A. Lemaitre, M. P. Almeida, P. Senellart, and A. G. White, Phys. Rev. Lett. **118**, 130503 (2017).

[24] C. P. Dietrich, A. Fiore, M. G. Thompson, M. Kamp, and S. Höfling, Laser Photonics Rev. **10**, 870 (2016).

[25] K. D. Jöns, U. Rengstl, M. Oster, F. Hargart, M. Heldmaier, S. Bounouar, S. M. Ulrich, M. Jetter, and P. Michler, J. Phys. D **48**, 085101 (2015).

[26] A. Enderlin, Y. Ota, R. Ohta, N. Kumagai, S. Ishida, S. Iwamoto, and Y. Arakawa, Phys. Rev. B **86**, 075314 (2012).

[27] A. Schwagmann, S. Kalliakos, I. Farrer, J. P. Griffiths, G. A. C. Jones, D. A. Ritchie, and A. J. Shields, Appl. Phys. Lett. **99**, 261108 (2011).

[28] M. Arcari, I. Söllner, A. Javadi, S. Lindskov Hansen, S. Mahmoodian, J. Liu, H. Thyrrestrup, E. H. Lee, J. D. Song, S. Stobbe, and P. Lodahl, Phys. Rev. Lett. **113**, 093603 (2014).

[29] G. Reithmaier, M. Kaniber, F. Flassig, S. Lichtmannecker, K. Müller, A. Andrejew, J. Vučković, R. Gross, and J. J. Finley, Nano Lett. **15**, 5208 (2015).

[30] M. Davanco, J. Liu, L. Sapienza, C.-Z. Zhang, J. V. De Miranda Cardoso, V. Verma, R. Mirin, S. W. Nam, L. Liu, and K. Srinivasan, Nat. Commun. **8**, 889 (2017).

[31] A. W. Elshaari, I. E. Zadeh, A. Fognini, M. E. Reimer, D. Dalacu, P. J. Poole, V. Zwiller, and K. D. Jöns, Nat. Commun. **8**, 379 (2017).

[32] J.-H. Kim, S. Aghaeimeibodi, C. J. K. Richardson, R. P. Leavitt, D. Englund, and E. Waks, Nano Lett. **17**, 7394 (2017).

[33] L. Midolo, S. L. Hansen, W. Zhang, C. Papon, R. Schott, A. Ludwig, A. D. Wieck, P. Lodahl, and S. Stobbe, Opt. Express **25**, 33514 (2017).

[34] J. Wang, A. Santamato, P. Jiang, D. Bonneau, E. Engin, J. W. Silverstone, M. Lermer, J. Beetz, M. Kamp, S. Höfling, M. G. Tanner, C. M. Natarajan, R. H. Hadfield, S. N. Dorenbos, V. Zwiller, J. L. O'Brien, and M. G. Thompson, Opt. Commun. **327**, 49 (2014).

[35] N. Prtljaga, R. J. Coles, J. O'Hara, B. Royall, E. Clarke, A. M. Fox, and M. S. Skolnick, Appl. Phys. Lett. **104**, 231107 (2014).

[36] N. C. Harris, D. Grassani, A. Simbula, M. Pant, M. Galli, T. Baehr-Jones, M. Hochberg, D. Englund, D. Bajoni, and C. Galland, Phys. Rev. X **4**, 041047 (2014).

[37] M. Kaniber, F. Flassig, G. Reithmaier, R. Gross, and J. J. Finley, Appl. Phys. B **122**, 115 (2016).

[38] T. Lund-Hansen, S. Stobbe, B. Julsgaard, H. Thyrrestrup, T. Sünner, M. Kamp, A. Forchel, and P. Lodahl, Phys. Rev. Lett. **101**, 113903 (2008).

[39] P. Stepanov, A. Delga, X. Zang, J. Bleuse, E. Dupuy, E. Peinke, P. Lalanne, J.-M. Gérard, and J. Claudon, Appl. Phys. Lett. **106**, 041112 (2015).

[40] M. N. Makhonin, J. E. Dixon, R. J. Coles, B. Royall, I. J. Luxmoore, E. Clarke, M. Hugues, M. S. Skolnick, and A. M. Fox, Nano Lett. **14**, 6997 (2014).

[41] S. Kalliakos, Y. Brody, A. J. Bennett, D. J. P. Ellis, J. Skiba-Szymanska, I. Farrer, J. P. Griffiths, D. A. Ritchie, and A. J. Shields, Appl. Phys. Lett. **109**, 151112 (2016).

[42] M. Schwartz, U. Rengstl, T. Herzog, M. Paul, J. Kettler, S. L. Portalupi, M. Jetter, and P. Michler, Opt. Express **24**, 3089 (2016).

[43] F. Liu, A. J. Brash, J. O'Hara, L. M. P. P. Martins, C. L. Phillips, R. J. Coles, B. Royall, E. Clarke, C. Bentham, N. Prtljaga, I. E. Itskevich, L. R. Wilson, M. S. Skolnick, and A. M. Fox, Nat. Nanotechnol. **13**, 835 (2018).

[44] J.-W. Pan, Z.-B. Chen, C.-Y. Lu, H. Weinfurter, A. Zeilinger, and M. Żukowski, Rev. Mod. Phys. **84**, 777 (2012).

[45] D. Press, K. De Greve, P. L. McMahon, T. D. Ladd, B. Friess, C. Schneider, M. Kamp, S. Höfling, A. Forchel, and Y. Yamamoto, Nat. Photonics **4**, 367 (2010).

[46] A. Majumdar, E. D. Kim, and J. Vučković, Phys. Rev. B **84**, 195304 (2011).

[47] J. Iles-Smith, D. P. S. McCutcheon, A. Nazir, and J. Mørk, Nat. Photonics **11**, 521 (2017).

[48] See Supplemental Material at http://link.aps.org/supplemental/10.1103/PhysRevLett.122.173602 for further experimental details, simulation results, and description of the two-photon interference histograms.

[49] J. Förstner, C. Weber, J. Danckwerts, and A. Knorr, Phys. Rev. Lett. **91**, 127401 (2003).

[50] L. Hanschke, K. A. Fischer, S. Appel, D. Lukin, J. Wierzbowski, S. Sun, R. Trivedi, J. Vučković, J. J. Finley, and K. Müller, Quantum Inf. **4**, 43 (2018).

[51] A. G. Fowler, A. M. Stephens, and P. Groszkowski, Phys. Rev. A **80**, 052312 (2009).

[52] E. Knill, Nature (London) **434**, 39 (2005).

[53] Y.-J. Wei, Y.-M. He, M.-C. Chen, Y.-N. Hu, Y. He, D. Wu, C. Schneider, M. Kamp, S. Höfling, C.-Y. Lu, and J.-W. Pan, Nano Lett. **14**, 6515 (2014).

[54] M. Varnava, D. E. Browne, and T. Rudolph, Phys. Rev. Lett. **100**, 060502 (2008).

[55] X.-L. Wang, L.-K. Chen, W. Li, H.-L. Huang, C. Liu, C. Chen, Y.-H. Luo, Z.-E. Su, D. Wu, Z.-D. Li, H. Lu, Y. Hu, X. Jiang, C.-Z. Peng, L. Li, N.-L. Liu, Y.-A. Chen, C.-Y. Lu, and J.-W. Pan, Phys. Rev. Lett. **117**, 210502 (2016).

[56] F. Kaneda and P. G. Kwiat, arXiv:1803.04803.

[57] J. Carolan, C. Harrold, C. Sparrow, E. Martín-López, N. J. Russell, J. W. Silverstone, P. J. Shadbolt, N. Matsuda, M. Oguma, M. Itoh, G. D. Marshall, M. G. Thompson, J. C. F. Matthews, T. Hashimoto, J. L. O'Brien, and A. Laing, Science **349**, 711 (2015).